

Design of Setups for Plasma Propulsion Plume Experiments

A Major Qualifying Project Report

Submitted to the Faculty

of the

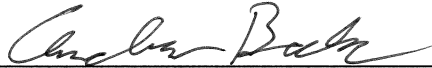
WORCESTER POLYTECHNIC INSTITUTE

in partial fulfillment of the requirements for the

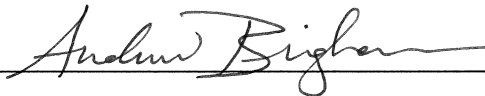
Degree of Bachelor of Science

in Aerospace Engineering

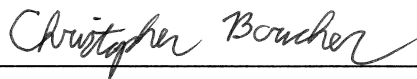
by



Andrew Baker



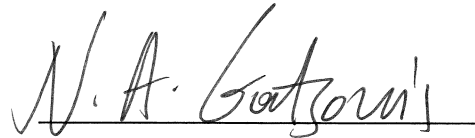
Andrew Bingham



Christopher Boucher

March 1, 2012

Approved:



Professor Nikolaos A. Gatsonis, Advisor
Mechanical Engineering Department, WPI

Abstract

The project involves design, analysis and fabrication of setups to be used in experiments with plasma plumes from electric micropropulsion devices. The setup for a 1.25m-diameter 1.845m-long large vacuum chamber includes a fixed plasma-source stand and a translating plasma-diagnostics stand. Design and structural analysis are performed using Solidworks and COMSOL Multiphysics. The setup for a 0.57m- diameter, 0.55m-long small vacuum chamber includes a plasma-diagnostics stand placed on a manual translation table along the plume axis. The realized design involves motorized transverse and rotary stages to align a Langmuir probe with the direction of the ion plume flow. Estimates of plume properties needed for probe sizing are obtained with simulations using a particle-in-cell plasma code.

Acknowledgements

We would like to express our deepest appreciation for the close attention Professor Nikolaos Gatsonis paid to our design iterations, assembly, report writing, and general understanding of the material covered in this Major Qualifying Project. We would also like to extend our gratitude to Michael Morin, a graduate advisee of Professor Gatsonis, for his assistance throughout the design process all the way to integration. Without their guidance and persistent help this project would not have been possible.

We would also like to thank Professor Gatsonis and Worcester Polytechnic Institute for providing us with state of the art equipment and facilities. The use of vacuum chambers, mills, and design laboratories were absolutely necessary in the completion of this project. Without the support of this Institution to further the education of all of its undergraduates, we would not have been able to put theory into practice.

Authorship

| <u>Section</u> | <u>Author</u> |
|-------------------------------------|----------------------|
| Chapter 1 Introduction, 1.1, 1.2 | AJB, ANB, CB |
| Chapter 2 2.1, 2.2 | AJB |
| Chapter 3 3.1, 3.2, 3.3, 3.4 | ANB |
| Chapter 4 | CB |
| Chapter 5 5.1 | AJB, ANB, CB |
| Appendix | CB |
| References | AJB, ANB, CB |

Table of Contents

| | |
|-------------------------------------------------------------------------------|----|
| Abstract..... | 2 |
| Acknowledgements | 3 |
| Authorship..... | 4 |
| List of Figures..... | 6 |
| List of Tables..... | 8 |
| Chapter 1: Background, Objectives, and Design Approach..... | 9 |
| Introduction | 9 |
| 1.1 Review of Vacuum Facilities, Plasma Diagnostics, and Plasma Source | 10 |
| 1.2 Objectives, Design Approach and Methods..... | 12 |
| Chapter 2: Horizontal Translation Table for Large Vacuum Facility | 14 |
| 2.1 Design Criteria and Objectives | 14 |
| 2.2 Equipment, Materials and Construction | 17 |
| Chapter 3: Source Stand and Translation Table for Small Vacuum Facility | 22 |
| 3.1 Design Criteria and Objectives | 22 |
| 3.2 Design of Translation Table..... | 24 |
| 3.3 Cost Analysis | 37 |
| 3.4 Vacuum Pump Characteristics | 38 |
| Chapter 4: Ion Source Plume Modeling | 42 |
| 4.1 PLUMPIC Simulation of the Ion Source | 42 |
| Chapter 5: Conclusions & Recommendations..... | 49 |
| 5.1 Recommendations | 51 |
| Appendix | 53 |
| References..... | 57 |

List of Figures

| | |
|------------------------------------------------------------------------------------------------------------------------------------------------------------------------------------------------------------------------------------------------------------------------------|----|
| Fig. 2.1: CAD model of the large vacuum chamber displaying the T-slotted rails, outlets, and viewing window..... | 15 |
| Fig. 2.2: An illustration of the range in which measurements may be taken using the proposed design for the Large Vacuum Facility. Here θ is the beam divergence angle..... | 17 |
| Fig. 2.3: Threaded flange for $\frac{3}{4}$ inch fitted hollow pipe mounting. (McMaster) | 19 |
| Fig. 2.4: Wing nut and screw attachment allowing for manual vertical movement..... | 19 |
| Fig. 2.5: Isometric view of the final design. | 20 |
| Fig. 3.1: Opened bell-jar | 24 |
| Fig. 3.2: Partridge’s Thruster/TLP Orientation, surrounded by a Faraday Cage to limit EMI, which could corrupt measurements. | 25 |
| Fig. 3.3: Orientation of stages within the bell-jar..... | 26 |
| Fig. 3.4: Stress and strain analysis performed on the first iteration of the translation table design.. | 27 |
| Fig. 3.5: Stress distribution in the second iteration of the translation table design. Fig. 3.5a shows the stress distribution for the entire structure, whereas Fig. 3.5b illustrates the heightened stress adjacent to the supporting beams in the structure..... | 28 |
| Fig. 3.6: Displacement field for the third iteration of the translation table design. Maximum predicted deformation is approximately 57 microns..... | 29 |
| Fig. 3.7: Cross section of Upright Guide Rails..... | 30 |
| Fig. 3.8: Equivalent simplified Guide Rail..... | 31 |
| Fig. 3.9: Displacement field for the fourth iteration of translation table design. | 31 |
| Fig. 3.10: Penultimate concept design. Note the inclusion of the false bottom. | 32 |
| Fig. 3.11: Displacement field for the fourth iteration of the translation table design. Maximum predicted deformation is approximately 0.87 microns..... | 33 |
| Fig. 3.12: Final Translation Table iteration | 34 |
| Fig. 3.13 (a, b, c): Dynamic loading | 35 |
| Fig. 3.14: Final design..... | 36 |
| Fig. 3.15: Vector plot of CEX current density in a half-domain surrounding the electric thruster, which has an exit centered at (0.5m, 0.0m). | 44 |
| Fig. 3.16: A close-up view of the thruster exit from Fig. 3.15. Note that CEX ions generated due to collisions immediately beyond the accelerator grid are more likely to be deflected toward the grid than away from it, unlike ions generated in more distant regions..... | 44 |
| Fig. 3.17: Axial component of current density across the thruster exit, shown with a sample quartic fit generated using MATLAB’s <i>polyfit</i> routine. | 45 |

Fig. 3.18: Common logarithm of ion collision frequency in a half-domain immediately surrounding the ion source. Note a sharp spike located at the center of the thruster exit. 45

Fig. 3.19: CEX backflow current at various iterations of *plumpic*. The backflow current easily reaches steady state before the 1000th iteration. 46

List of Tables

| | |
|-------------------------------------------------------------------------------------------------------------|----|
| Table 2.1: Cost breakdown for all components required for construction of downstairs translation table..... | 21 |
| Table 3.1: Cost Analysis for Upstairs Translation Table..... | 38 |

Chapter 1: Background, Objectives, and Design Approach

Introduction

Electric propulsion systems, by virtue of their ability to achieve remarkably high exhaust velocities, are one of the most efficient means of spacecraft propulsion. They are unique among all types of thrusters for the extremely high specific impulses they can deliver (I_{sp}) which translates into impressive fuel efficiency. Such a combination causes electric propulsion to be a central factor in the ability to carry out missions requiring large velocity changes, such as interplanetary travel, as well as missions requiring very low propellant masses, including several applications in attitude control and station-keeping. However, their characteristic low thrust-to-power ratios prevent electric propulsion systems from providing an effective means of liftoff or other impulsive maneuvers.

Electric thrusters may be broken down into three categories, which are not entirely mutually exclusive: electrothermal, electrostatic, and electromagnetic. Electrothermal thrusters use electricity to heat a propellant gas and expel it through a nozzle, with specific impulses typically varying between 200 and 1000 seconds. Electrostatic thrusters use electric fields to accelerate ions to extremely high velocities and expel them through a charged grid, with specific impulses between 1500 and 8000 seconds. Electromagnetic thrusters accelerate a propellant using a combination of electric and magnetic fields, and generally have specific impulses between 600 and 5000 seconds. All three types of electric thruster have thrust values in the millinewton range, emphasizing the impracticality of such thrusters for missions requiring large velocity changes over small time scales, such as liftoff (Sutton).

While electric thrusters are inadequate for a mission requiring high acceleration, they excel at providing a large velocity boost over an extended period of time, generally many months of continuous operation. Therefore, improvements in the reliability, efficiency, and operating lifetime of electric thrusters are among the primary concerns of aerospace engineers.

The goal of our MQP is to develop and implement experimental setups that allow development of plasma diagnostics that are used in the investigation of plumes of electric thrusters. The MQP focuses on triple Langmuir probes, quadruple Langmuir probes, and a micro retarding potential analyzer. The plasma source and probe positioning systems are to be implemented in WPI's Large Vacuum Facility located in HL016 and in the Small Vacuum Facility under construction in HL314.

1.1 Review of Vacuum Facilities, Plasma Diagnostics, and Plasma Source

The Large Vacuum facility in HL016 has a cylindrical vacuum chamber which has a 1250mm diameter and is 1845mm long. The Small Vacuum facility in HL314 consists of a bell jar with a maximum height of 550mm and a diameter of 570mm. The domed top of the bell jar, however, restricts the utilization of a small part of this vertical space. The bell-jar is evacuated via a VHS-6 diffusion pump with an extended cold cap. The chamber has an advertised pumping speed of 1600 L/s for air, or 2000 L/s for helium; since the propellant used in our Kaufman ion source, argon, has a greater molecular weight than either helium or diatomic nitrogen, the effective pumping rate in the chamber can be expected to be slightly lower than the advertised pumping rate, even under ideal conditions.

The ultimate purpose of the MQP is to design an apparatus and a testing method capable of measuring the electron temperature and ion number density of a pulsed plasma thruster. The method will be developed via tests employing a 3-cm Kaufman ion source before any PPT is used.

The plume of an electric thruster contains several components which behave in distinct ways. The actual thrust is produced by fast-moving ions, often at velocities of 10 km/s or higher, which have been accelerated by electromagnetic forces. In addition, the plasma contains neutral particles which have been accelerated thermally. Slow-moving ions are also generated through charge-exchange collisions between fast-moving ions and slower neutrals. Electrons, used to neutralize the outgoing plasma stream, also play a significant role in the plasma's behavior, and are necessary to maintain electric neutrality of the spacecraft. Finally, sputtering can cause particles from the equipment to enter the plume; these particles are collectively referred to as Non-Propellant Efflux, or NPE (Roy 54).

To measure the plumes from a PPT, Triple Langmuir Probes (TLPs) and a micro-Retarding Potential Analyzer (RPA) will be designed and fabricated. To ensure accuracy and reproducibility of the probe's measurements, a positioning mechanism will be designed and constructed, consisting of two linear degrees of freedom and one rotational degree of freedom. The design of the positioning system, or translation table, must be flexible enough to allow the TLP to be removed and replaced with an existing micro-Retarding Potential Analyzer (RPA). After fabrication of the probes and translation table are complete, a series of measurements will be performed to obtain a profile of the electron

temperature, beam ion density, and direction of plasma flow at various positions relative to the thruster.

1.2 Objectives, Design Approach and Methods

The first objective of the MQP is to Design a translation table for the large vacuum chamber in the basement of Higgins Laboratories.

- **Requirements:** Implementing two translational degrees of freedom and one rotational degree of freedom, the design should enable the TLP or micro-RPA to reach the largest possible amount of space within the substantially large vacuum chamber.
- **Approach and Methods:** Given the aforementioned chamber dimensions, seek the commercially available linear stages which offer the greatest possible range of motion in a vacuum environment for a reasonable cost. While price and linear range are the most prominent figures of merit in the design of a positioning system for the Large Vacuum Facility, positioning accuracies on the order of hundreds of microns or less are desired for the two linear stages.

The second major objective is to Design a translation table for the Small Vacuum Facility (SVF) in HL314.

- **Requirements:** Implement two translational degrees of freedom and one rotational degree of freedom. Design must be oriented vertically in order to utilize the largest possible amount of empty space within the bell-jar. Unlike the design for the Large Vacuum Facility, positioning accuracy is a considerable figure of merit in the design of the positioning system for the Small Vacuum Facility, since diagnostics will be

performed over smaller length scales. Accuracy on the order of several tens of microns is preferred.

- Approach: Use SolidWorks to generate a three-dimensional model of the positioning system. Import the model into COMSOL Multiphysics Ver. 4.2 and simulate the deformation in the stages in both static and dynamic loading situations. Iteratively reinforce the design of the positioning system until deformations are at least a full order of magnitude less than the uncertainty in the positioning of the linear stages.
- Run simulations to ensure that the bell-jar can provide an acceptable operating environment for a 3-cm Kaufman ion source. The simulation will also provide an *a priori* estimate of certain ion beam parameters, which will aid in TLP design, particularly in sizing the probe wires.

Chapter 2: Horizontal Translation Table for Large Vacuum Facility

In this chapter, we present the design for a translation table to be implemented in WPI's Large Vacuum Facility located in HL016. The chapter will include the orientation of the table with respect to the vacuum chamber, a description of all parts necessary for assembly, and a cost analysis of these parts. It will further examine the objectives of the translational motions and how they will be achieved.

2.1 Design Criteria and Objectives

The large vacuum chamber has a cylindrical shape with the end caps facing the user. To utilize the greatest possible range of motion with two linear stages, the translation table design will incorporate a 1 meter stage oriented horizontally, parallel to the centerline of the chamber, and a 0.5 meter stage, oriented horizontally perpendicular to the first. The translation table will be built upon existing T-slotted rails, which are mounted to the bottom and separated by a distance of $\frac{1}{2}$ -m. These rails provide the initial support for the entire translation table structure. The vacuum chamber also provides the user with several outlets for power and any motion adjustments. This will allow wires for the TLP, rotary stage, and two linear stages to run outside of the chamber while maintaining a vacuum. Fig. 2.1 displays a CAD model of the large vacuum chamber and the T-slotted rails as previously described.

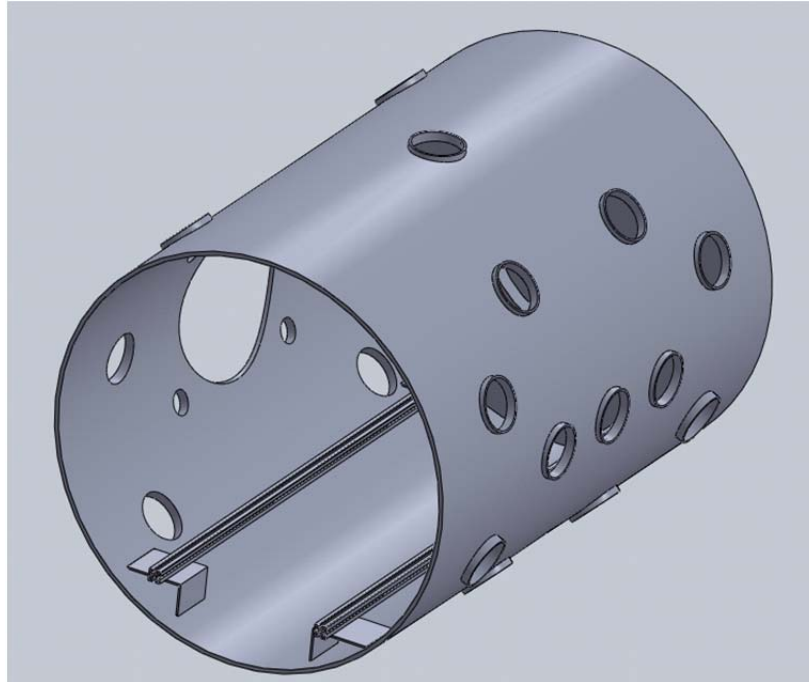


Fig. 2.1: CAD model of the large vacuum chamber displaying the T-slotted rails, outlets, and viewing window.

The translation table must be capable of positioning a TLP, QLP or the micro-RPA within the horizontal plane containing the centerline of the plasma thruster exit, in both the axial and transverse directions. In addition to two-dimensional linear motion, the probe must be able to rotate about an axis normal to the transverse-axial plane, in order to orient itself in the direction which yields maximum probe current, which corresponds to the direction of maximum plasma flow. All three degrees of freedom must also be mechanically driven and controlled from outside of the vacuum chamber in real time. The design must also allow for all three movements simultaneously and should minimize cost while utilizing the maximum possible range of motion allowed within the vacuum chamber.

Initially, the objective was to implement an existing vacuum-rated translation table, and to retrofit a TLP and RPA to the existing table. After a thorough inventory of all available materials, it became apparent that nothing offered the long ranges or the three degrees of freedom needed to fully take advantage of the vacuum chamber's size. Although an existing table, which fulfilled some of the design requirements, was available, it lacked the ability to rotate the probe stand. Furthermore, the position on the existing translation table could only be adjusted manually. In order to move the probe, the vacuum chamber would need to be evacuated, and the plasma thruster would need to be activated once for every desired position and orientation of the TLP. Each repositioning of the probe would require several days. After further considering the magnitude of modifications that would be necessary, the decision was made to abandon the existing table and to proceed by building a custom design that will perform the desired operations.

The custom design requires the purchase of three independent stages, two linear and one rotational. The two linear stages will allow for translation by one meter in the axial direction and one half meter in the transverse direction. The resolution of the tables available for purchase is on the order of microns, far smaller than the millimeter accuracy required for the positioning system.

The design will place the TLP/QLP or micro-RPA on top of a rotating platform to orient the probe parallel to the plasma flow. The rotary stage will then be mounted on the half-meter linear translational motor that will move perpendicular to the thruster exit centerline. Finally, the half-meter stage will be mounted on the 1-meter linear translational motor, which runs parallel to the centerline. This will allow us to move the probe in and out of the thruster's plume. The custom design will allow the user to completely remove the

entire test stand as one single component. Fig. 2.2 illustrates the range of the positioning system, with the regions dominated by beam ions and charge exchange ions clearly labeled.

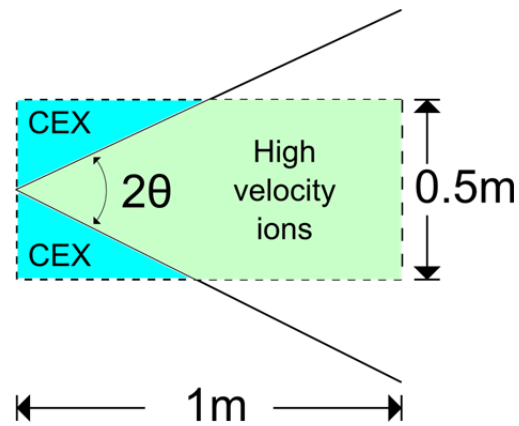


Fig. 2.2: An illustration of the range in which measurements may be taken using the proposed design for the Large Vacuum Facility. Here θ is the beam divergence angle.

2.2 Equipment, Materials and Construction

The required parts for complete construction of the custom design include the three motorized stages, the 406XR Axial Linear Stage, the 404XR Transverse Linear Stage, and the 200RT Rotary Stage (Parker). The design also requires 4 T-Slotted rails, two of which should reach 1 meter in length and the other two spanning a half-meter. The half-meter stage will be supported by two T-slotted rails at either end running directly parallel to the one meter stage. The half-meter rails should run parallel to the half meter stage, supporting the rotational stage. Mounted to the rotational stage via pipe flange, as seen in Fig. 2.3, will be the $\frac{3}{4}$ inch hollow aluminum piping. The pipe will also require a single hole, approximately $\frac{1}{4}$ inch diameter, to be drilled on the side directly opposite the side facing the thruster source. The hole and piping will shield the TLP/micro-RPA wires from the beam ions. Attached to one end of the one-meter T-Slotted rails will be the flat aluminum

plate to which the thruster stand will be mounted. The thruster stand is composed of a single strut channel and a hollow square tube equipped with a wing nut and screw connection as seen in Fig. 2.4. This hollow square tube will be permitted to slide up and down in the strut channel, as seen in Fig. 2.5, in order to adjust the height of thruster source in relation to the TLP/micro-RPA. The final assembly requirements are two fitted aluminum bases each mounted to the ends of the one-meter T-Slotted rails connecting the two rails and allowing the one-meter translation stage to rest. The final design can be seen in Fig. 2.5.

The materials for this custom design are mostly aluminum and lightweight. In searching for the components that would best fit the design, most could be located and purchased from McMaster Company. Table 2.1 shows the cost breakdown for each of the individual parts and a total cost estimate. It should be taken into consideration that the costs for all three translational stages do not reflect the additional cost of vacuum treatment. It should also be taken into consideration that some of the parts were estimated to be free of cost based on their availability of being located on site at Worcester Polytechnic Institute.

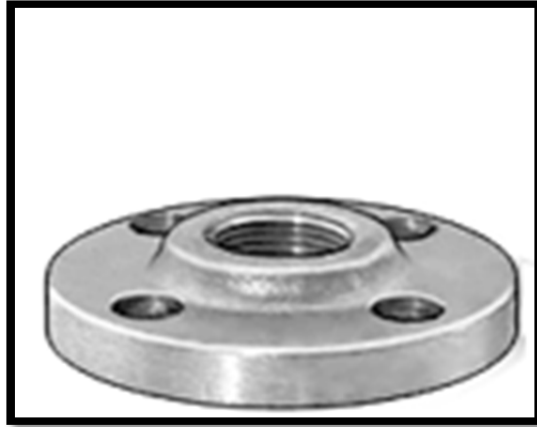


Fig. 2.3: Threaded flange for $\frac{3}{4}$ inch fitted hollow pipe mounting. (McMaster)

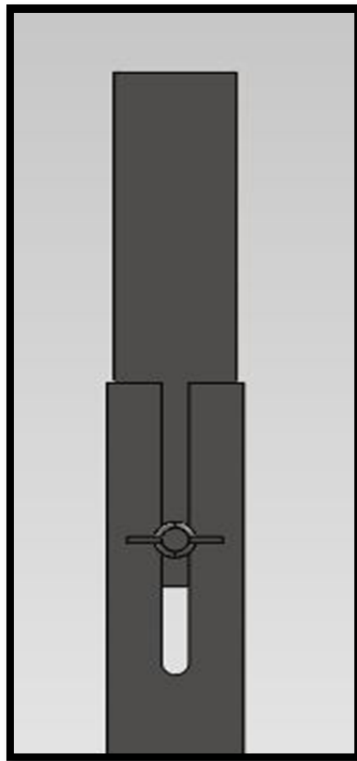


Fig. 2.4: Wing nut and screw attachment allowing for manual vertical movement.

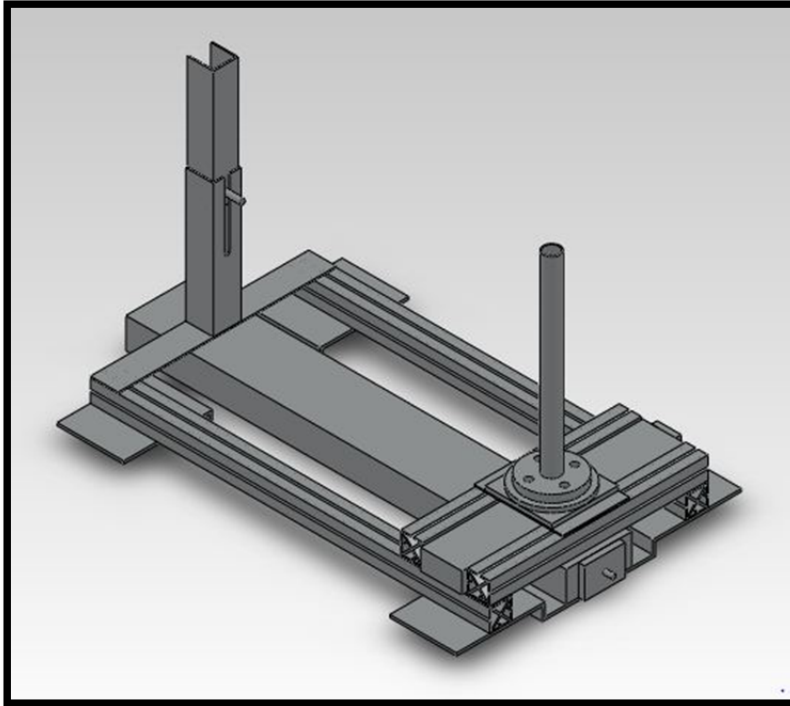


Fig. 2.5: Isometric view of the final design.

| Item | Quantity | Cost |
|-------------------------------|----------|--------|
| ½ Meter stage | 1 | 2819 |
| 1 Meter stage | 1 | 5106 |
| Rotary Stage | 1 | 2861 |
| 4' T Slotted Rail | 2 | 28.4 |
| 2' T Slotted Rail | 2 | 16.7 |
| 4 " Single Flange Guide Block | 8 | 446.88 |
| Aluminum L-Bracket | 4 | 0 |
| Flat Aluminum Plate | 1 | 0 |
| Hollow Piping | 1 | 54.36 |
| Strut Channel | 1 | 10.72 |
| Square Tubing (fitting) | 1 | 9.56 |

| | | |
|---------|--------------|-------------------|
| Bolts | 2 | 0 |
| Washers | 2 | 0 |
| | Total | \$11352.62 |

Table 2.1: Cost breakdown for all components required for construction of downstairs translation table.

Chapter 3: Source Stand and Translation Table for Small Vacuum Facility

In this chapter we present our work in adapting the methodology discussed in Chapter 2 to fit a smaller vacuum chamber. In place of purchasing three new stages, we employed two existing stages, one linear and one rotary. These stages were implemented such that the need of a third larger linear stage was deferred until more funds are procured. This deferment, however, led to an increased frequency in breaking the vacuum seal for manual adjustment of the stand. Thus we chose to use a smaller bell-jar vacuum chamber in HL 314 instead of the large chamber in the basement of Higgins Labs. This chamber requires much less time to bring to vacuum, and allows us to perform our experiments more efficiently.

3.1 Design Criteria and Objectives

As mentioned earlier, there are two vacuum chambers that were considered for the MQP. The large chamber, in the Vacuum Test Facility (VTF), located in the basement of Higgins Labs, is the 50 inch diameter, 72 inch long stainless steel vacuum chamber which will enable the creation of a vacuum environment for use in the characterization of electric and chemical thruster performance, investigation of neutral and ionized gas plume expansion in a vacuum, and testing of avionics for nanosatellites designed to operate in a vacuum environment.

The pumping system for the VTF includes a rotary mechanical pump, positive displacement blower combination capable of providing substantial pumping speed (> 560 liters/sec) at low vacuum (10^{-2} - 10^{-3} Torr). This pump pair can be used for tests requiring relatively high mass flow rates, such as plume measurements on micro-chemical thrusters.

For tests of electric thrusters where lower pressures (higher vacuum) are required, the mechanical pump would be used initially to pump the system down to the milli-Torr pressure range. Pumping would then transition to a 20" cryopump which can provide up to 10,000 liters/s (on N₂) at pressures less than 10⁻⁶ Torr (Gatsonis et al).

The Small Vacuum Facility is under development in HL 314. It consists of a bell-jar vacuum chamber with a VHS-6 diffusion pump with an extended cold cap. The pump has advertised pumping rates of 2000 L/s for helium or 1600 L/s for air. The bell-jar has a radius of 11.25 inch and a height of 32 inch, providing 12717 in³ of experimental volume. A probe stand and a translation table were designed for use in this bell-jar vacuum chamber, using a small linear stage and rotary stage which were left over from a previous MQP. As in the large vacuum chamber, the goal of translation table design for the bell-jar was to establish a TLP positioning system including two translation degrees of freedom and one rotational degree of freedom. The bell-jar became a more appealing choice for translation table construction than the large chamber in the basement due to its much lower construction cost. Fig. 3.1 below shows the bell-jar as it is opened for maintenance.

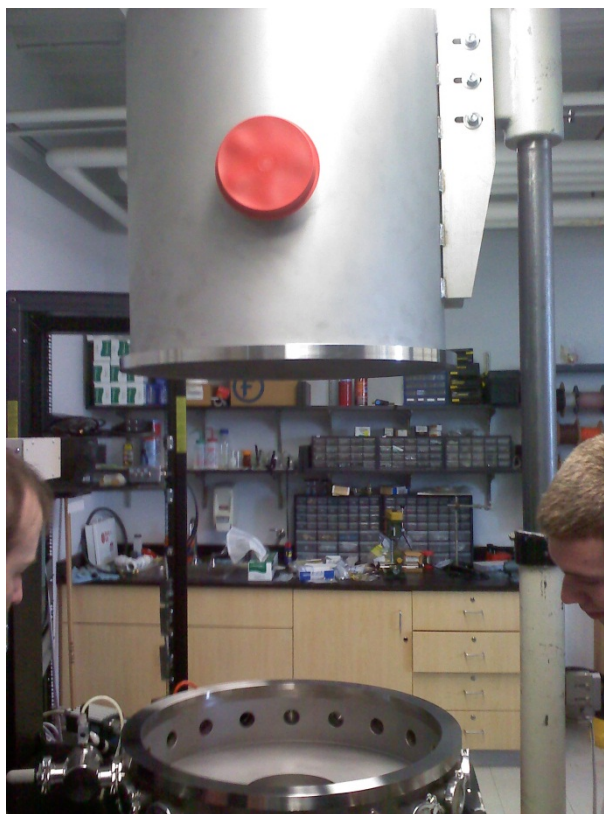


Fig. 3.1: Opened bell-jar

In contrast to the large vacuum chamber located in the basement of Higgins Laboratories, which requires approximately a day to cycle from atmospheric to vacuum conditions, the bell-jar upstairs can cycle much more quickly. In a few hours the jar can be loaded with the TLP or micro-RPA and brought to vacuum conditions, enabling faster data collection over a smaller range of positions than the vacuum chamber in the basement.

3.2 Design of Translation Table

The same bell-jar chamber was used to provide a vacuum environment with which to take measurements with a triple Langmuir probe on an Ion source (Partridge, 2007). The same two stages as discussed earlier were also used for his dissertation. Both stages

are controlled by stepper motors using a 2D polar sweep. Uncertainty in position of the linear stage (SN: 06050210) was limited by the motor step size. The ideal uncertainty in linear position was calculated by dividing the distance traveled per revolution by the steps per revolution, yielding an uncertainty of ± 20.0 micrometers. This value was increased to ± 40.0 micrometers though, because the motor might overshoot the desired steps by up to 1,000 steps. By the same approach and reasoning, the rotary stage (SN: 06050211) was calculated to have an uncertainty of $\pm 0.36^\circ$ (Partridge, 2007). The table and thruster can be seen in Fig. 3.2.

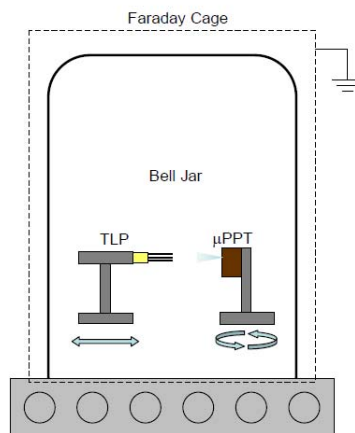


Fig. 3.2: Partridge's Thruster/TLP Orientation, surrounded by a Faraday Cage to limit EMI, which could corrupt measurements.

The micro pulsed plasma thruster (PPT) was mounted to the rotary stage, while the TLP was fixed to the linear stage. The two stages were fixed in position relative to each other, limiting the range of positions at which the TLP could take measurements relative to the PPT.

In order to obtain the greatest possible range of motion within the bell-jar, a vertically oriented translation table was designed. In the vertical translation table design, the ion source is mounted in the center of the base of the bell-jar, with its exhaust plume pointed directly upward. The TLP is mounted on a rotary stage, which is mounted on a linear stage oriented perpendicular to the centerline of the ion source. The rotary stage and small linear stage are secured by a pair of linear sliders to allow movement of the system in and out of the plume. Each block of the sliders may lock in position. The entire apparatus is then connected to a longer, vertical translational stage situated between a pair of vertical sliders, allowing the probe to be moved upward or downward at will. The entire design is illustrated by Fig. 3.3.

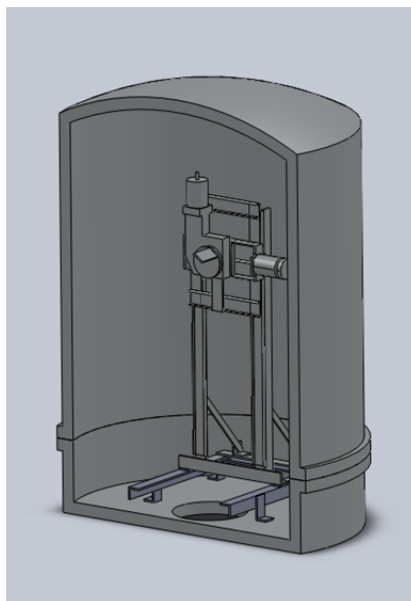


Fig. 3.3: Orientation of stages within the bell-jar.

Inside the bell-jar, a long vertical stage supports a much smaller horizontal stage, which in turn supports a rotary stage. A probe (TLP) attached to the rotary stage may then

be moved to an arbitrary point in the plane defined by the two linear stages, and rotated to orient itself with the ion flow. This orientation of the three translational stages and the TLP will be maintained through each of the design iterations.

To ensure that the translation table design is sufficiently stable, it was constructed in SolidWorks and imported into COMSOL Multiphysics. The first design of the translation table utilized a pair of angled beams to support the vertical slide rails as shown in Fig. 3.4. A body load of 24640 N/m^3 was applied to the structure to simulate the force of gravity on an all-aluminum structure.

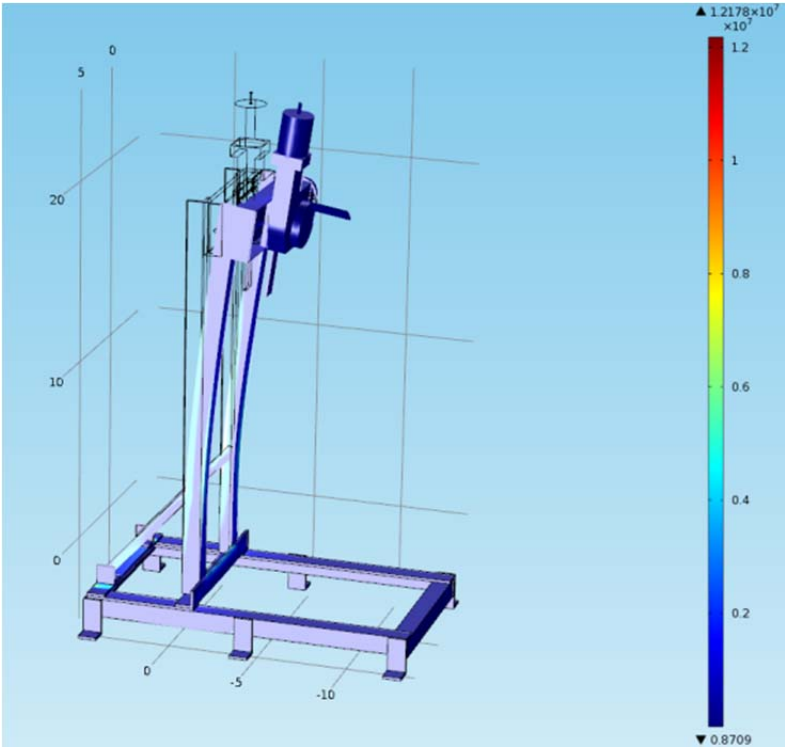


Fig. 3.4: Stress and strain analysis performed on the first iteration of the translation table design.

The first design was assumed to be composed of Al 2024. The structure was mainly composed of L cross-sectioned bars of 0.15 inch thickness. However, a finite element analysis of the design revealed that the magnitude of deflection experienced by the basic design, approximately 100 microns, would be unacceptable for the high-precision operation expected from the translation table.

The second iteration presented a structure made mostly of U cross-sectioned bars and an increased height of the back anchoring rail support. As illustrated in Fig. 3.5a and Fig. 3.5b, the maximum stress occurs at the base of the cross bar where this back support is attached. Fig. 3.6 illustrates a slightly improved design to Fig. 3.5 in that this location of high stress is made more robust.

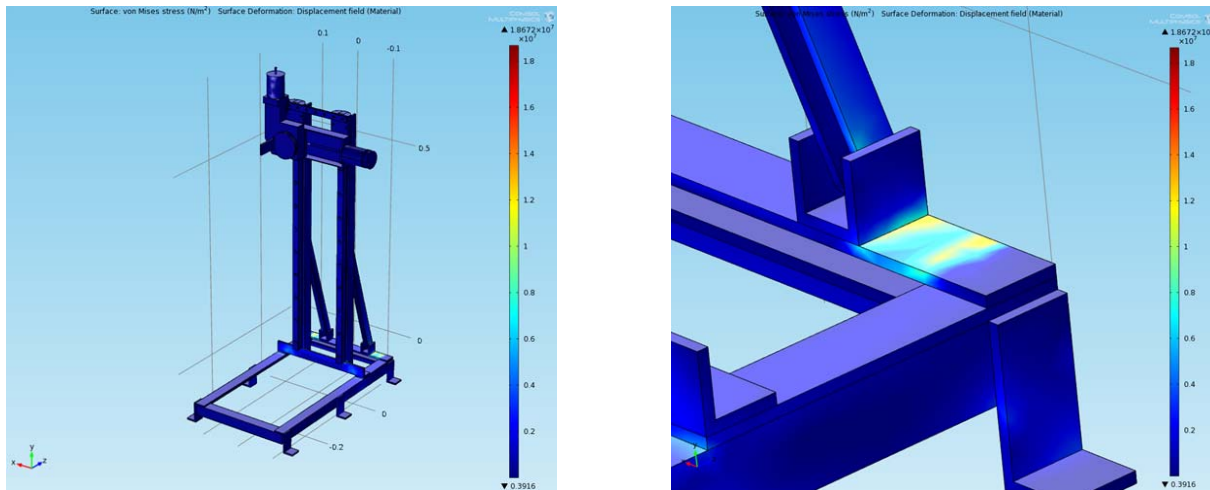


Fig. 3.5: Stress distribution in the second iteration of the translation table design. Fig. 3.5a shows the stress distribution for the entire structure, whereas Fig. 3.5b illustrates the heightened stress adjacent to the supporting beams in the structure.

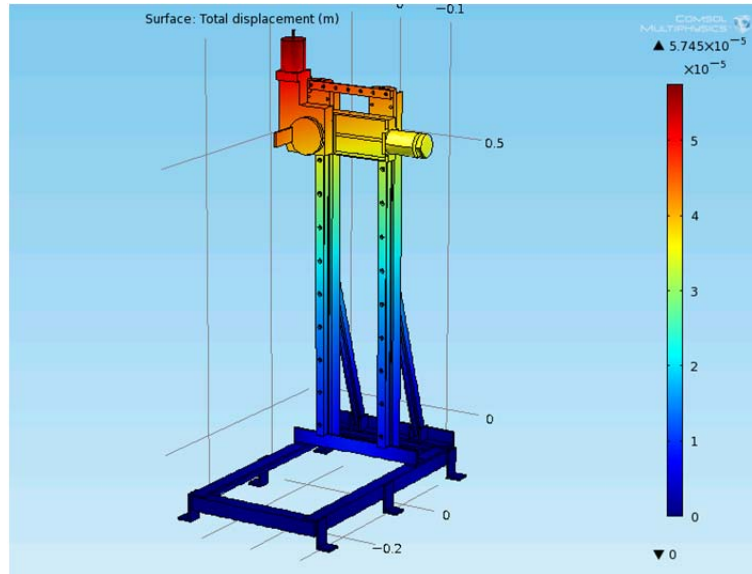


Fig. 3.6: Displacement field for the third iteration of the translation table design. Maximum predicted deformation is approximately 57 microns.

The design illustrated in Fig. 3.6 experienced a maximum displacement of 57.45 microns, on the same order of magnitude as the resolution of both stages. In order to further reduce the maximum deformation, a fourth iteration of the design was introduced.

Design analysis, as illustrated in Fig. 3.9, is complex enough to prevent it from being properly meshed on COMSOL when using 32 GB of RAM. Therefore, simplifications have been made to the design. The rectangular bars shown were T-slotted rails in the original design, which would not mesh properly, apparently due to lack of memory. The second moment of area of the T-slotted rail about a vertical axis running through its center was calculated as:

$$I_y = \int_{C.S.} x^2 dA,$$

where integration is performed over the entire cross-sectional area. To simulate the T-slotted rails using COMSOL in a manner which allowed the design to mesh properly, we designed a simplified cross section which possessed the same second moment of area.

Fig. 3.7 details the true geometry of the T-slotted rail cross section. The calculated moment of inertia that this rail possesses is $I=1.937\text{in}^4$.

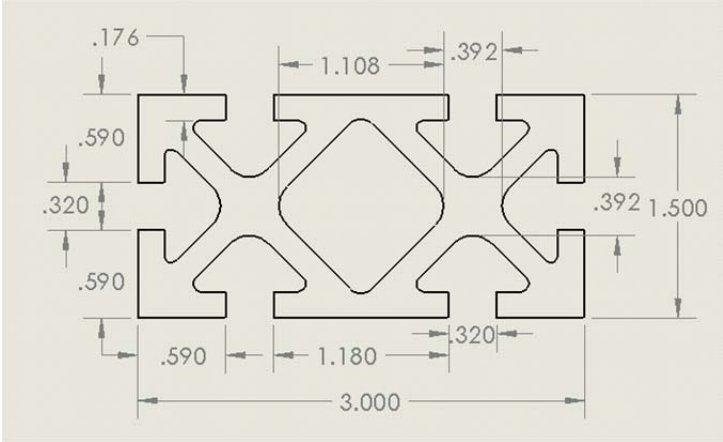


Fig. 3.7: Cross section of Upright Guide Rails

The simplified cross section, one which COMSOL was able to mesh, is a hollow rectangular prism as shown in Fig. 3.8 below. The thickness calculated that equated both moments of inertia was 0.227 inches on all four corners. The new cross-section has the same second moment of area about the vertical axis as the T-slotted rail. Although the structural integrity of the simplified cross-section is comparable to that of the T-slotted rail cross-section, a small increase in structure mass will result from the slightly increased area of the simplified model.

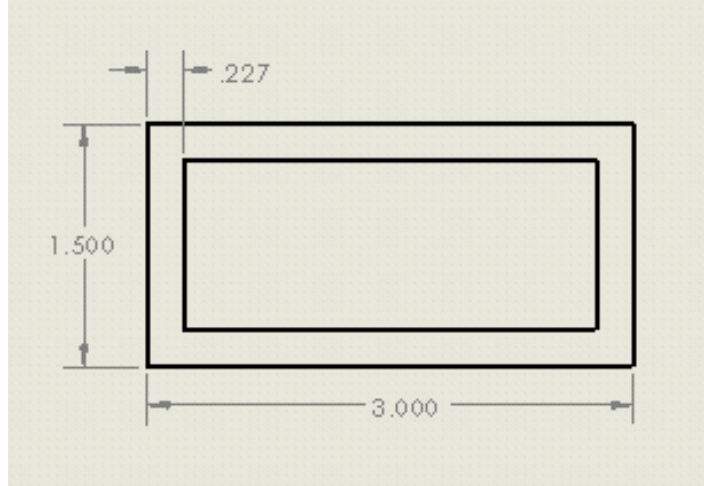


Fig. 3.8: Equivalent simplified Guide Rail

Below in Fig. 3.9 is the simplified version of our design iteration. The 24640 N/m^3 body force was applied according to procedure.

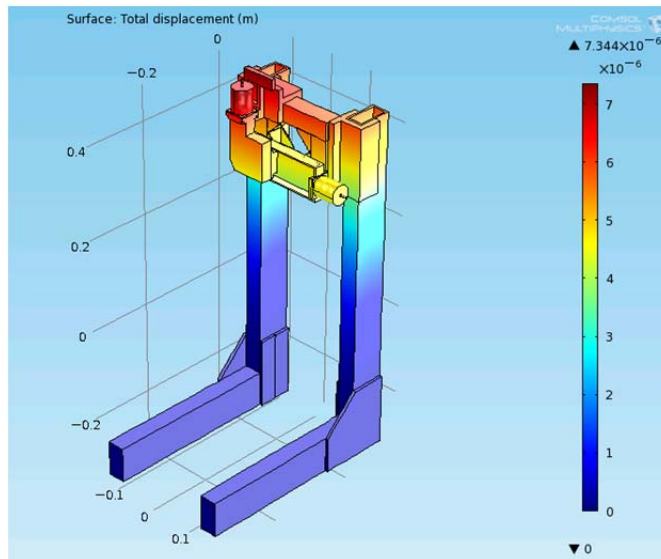


Fig. 3.9: Displacement field for the fourth iteration of translation table design.

The simplified structure of Fig. 3.9 yielded a maximum displacement of 7.344 microns. Displacement of the TLP mount was closer to 5 microns. The design in Fig. 3.9 will be fixed to a “false bottom,” a thin doughnut-shaped plate which will provide a mounting surface for the table. This false bottom is then placed inside the bell-jar to prevent any damage to the structure itself. The false bottom is illustrated in Fig. 3.10.

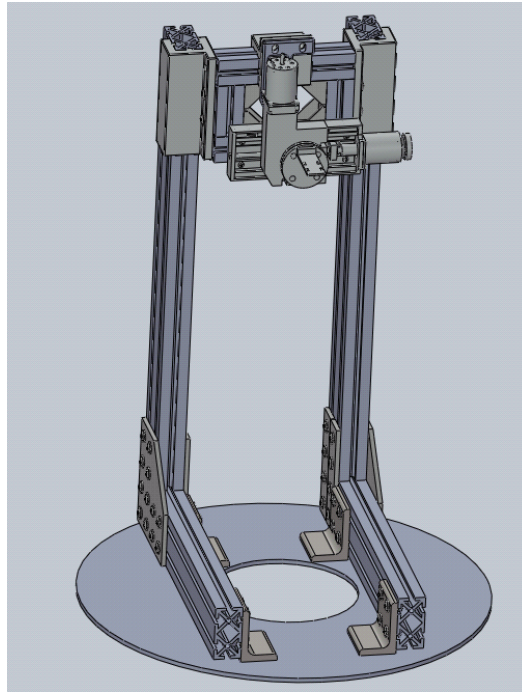


Fig. 3.10: Penultimate concept design. Note the inclusion of the false bottom.

Fig. 3.10, though the most stable yet, illustrated the need to build additional support in order to reduce static deflections to the sub-micron range. This desired deflection was due to the resolution of the TLP; having a high-resolution tool mounted to a low-resolution stage would limit the quality of experimental data.

The final design iteration involved creating a “cage” structure that added significant support and stability to the horizontal and rotary transition stages. Again, using the

equivalent simplified cross section upright support bars, we imported the design from SolidWorks to COMSOL and applied the body load.

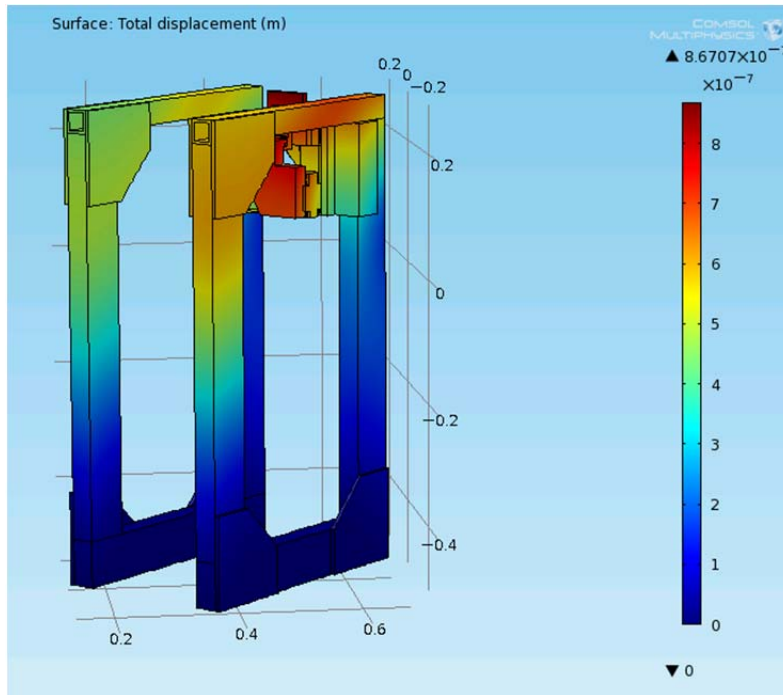


Fig. 3.11: Displacement field for the fourth iteration of the translation table design. Maximum predicted deformation is approximately 0.87 microns.

With the same body load applied to the cage structure, a maximum deflection of 0.87 microns was measured, and illustrated in Fig. 3.11. Static deflections less than one micron are acceptable for the probe positioning system.

Dynamic loading, simulating and measuring deflections of the structure by raising and lowering the horizontal and rotary stages, was our last design test we needed to perform before procuring all needed materials and building the structure. Fig. 3.12 displays our final simplified design iteration. Added to the cage were three 8.5 inch long support bars. These bars add support to the cage, stiffening it during dynamic loading.

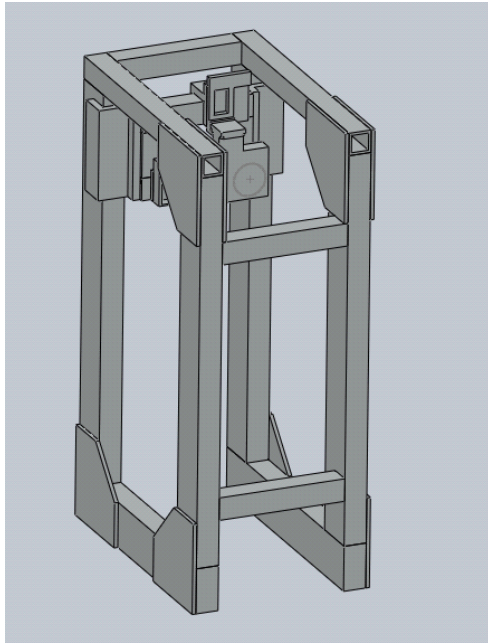
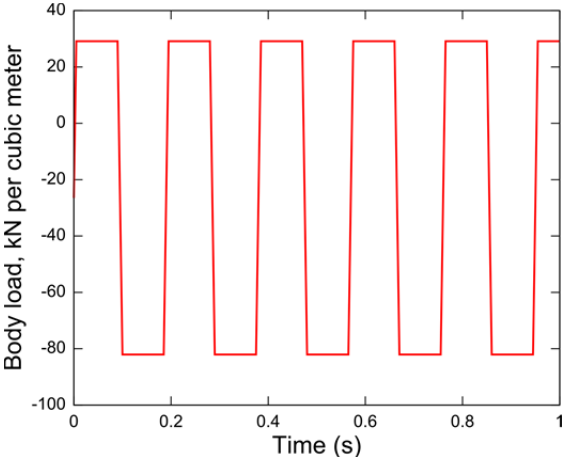


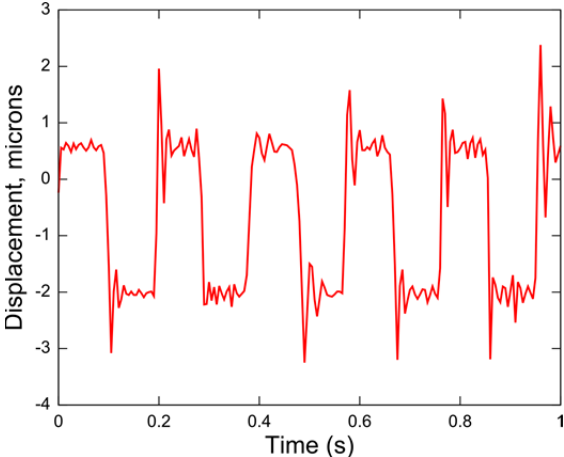
Fig. 3.12: Final Translation Table iteration

Dynamic loading in COMSOL involved raising and lowering the horizontal and rotary stages. To simulate the forces required to translate the horizontal stage up and down within the vacuum facility, a periodic body load was applied to the horizontal and rotary stages in COMSOL. Such a body load represents the force required to accelerate the stage to its maximum advertised upward velocity (Parker), then to decelerate the stage to zero velocity and accelerate it to its maximum downward velocity, then repeat this cycle. Such a periodic load represents the greatest possible abrupt change in body load which the positioning system can possibly experience during operation. Fig. 3.13a illustrates the square wave input pattern; note that the average of the upward and downward forces is negative because the body loads due to upward and downward acceleration are superimposed on a downward body load due to gravity. Fig. 3.13b illustrates the vertical deflection of the positioning system due to these periodic body loads; note that the vertical

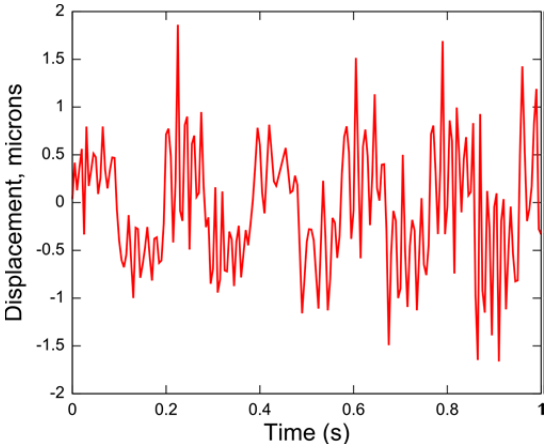
displacement has the same period as the square wave input, as expected, and that the combination of vertical deflections due to the stage weight and dynamic loading does not exceed 3 microns in either direction. The deflection illustrated in Fig. 3.13c is the simulated motion of the probe into and out of the plane containing both translational stages.



3.13a



3.13b



3.13c

Fig. 3.13 (a, b, c): Dynamic loading

The deflection in the transverse direction was a full order of magnitude smaller than either of the deflections shown in Fig. 3.13b and 3.13c. Thus, the maximum deflection expected to occur due to motion of the positioning system is less than 4 microns.

The final design is portrayed in Fig. 3.14 below. As illustrated, it is mounted to the false bottom, which was discussed earlier. The fourth 8.5 inch cross bar that is located at the bottom center of the structure, over the hole in the false bottom, is to be used for mounting the thruster (with plume ejecting upward) as well as any other system wiring or piping.

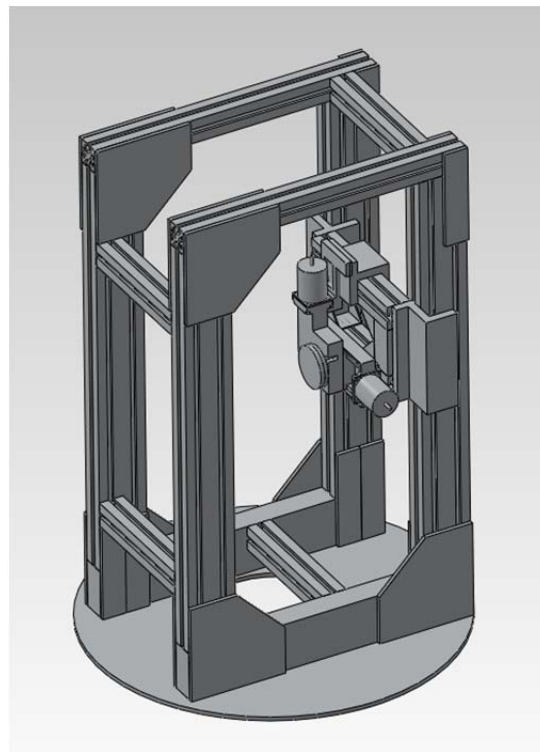


Fig. 3.14: Final design

3.3 Cost Analysis

The cost of each component for the bell-jar translation table is listed in Table 3.1. Note that the overall cost of the construction of the table is approximately one third of that for a translation table for the large vacuum chamber as illustrated in Table 2.1. Even if an extremely high-precision table is chosen for the bell-jar, the cost is still approximately half that of a translation table for the large chamber.

Investigation into these linear stages has highlighted two possible selections from AXIS New England, a local distributor of high precision linear and rotary stages from the Parker Hannifin Corporation. Depending on the desired accuracy and available funds, either the 402400XRMS_D3H1L1C3M3E1R1, for \$2744 and a position uncertainty of 40 μ m, or the 402400XRMP_D3H1L1C3M3E3R1, for \$5064 and a position uncertainty of 20 μ m, could be purchased. Even the less expensive of the two stages is more than double the cost of the entire structure thus far.

| Model or Part # | Item Description: | Qty: | Unit Price: | Total Price: |
|------------------|-----------------------------------------------------------------------------------------------|------|-------------|--------------|
| 47065T137 | Aluminum Inch T-Slotted Framing System Six-Slot Double, 1-1/2" Solid Extrusion, 4' Length | 4 | 50.25 | 201.00 |
| 47065T128 | Aluminum Inch T-Slotted Framing System Four-Slot Single, 1-1/2" Solid Extrusion, 6' Length | 1 | 42.58 | 42.58 |
| 5537T51 | 90 Deg Sngl Brace, for 1-1/2" & 40mm Extrusions | 6 | 7.98 | 47.88 |
| 47065T42 | Aluminum Inch T-Slotted Framing System Extended Plate, Single, 4-Hole for 1-1/2" Extrusion | 12 | 6.35 | 76.20 |
| 47065T178 | Aluminum Inch T-Slotted Framing System 90 Degree Plate, Single, 5-Hole, for 1-1/2" Extrusion | 8 | 7.76 | 62.08 |
| 47065T181 | Aluminum Inch T-Slotted Framing System 90 Degree Plate, Double, 12-Hole, for 1-1/2" Extrusion | 8 | 14.36 | 114.88 |
| 47065T97 | Std Zinc-Pltd STL End-Feed Fastener, for 1-1/2" Aluminum Inch T-Slotted Framing System | 6 | 2.71 | 16.26 |

| | | | | |
|------------------|--------------------------------------------------------------------------------------|----|-------|-------------------|
| 47065T149 | Double End-Feed Fastener, for 1-1/2" Aluminum Inch T-Slotted Framing System | 30 | 6.76 | 202.80 |
| 60585K33 | Linear Bearing for T-Slotted Framing for 1-1/2" Width Rail, Side-Mount, 2-13/16" L | 1 | 55.35 | 55.35 |
| 60585K34 | Linear Bearing for T-Slotted Framing for 1-1/2" Width Rail, Side-Mount, 6" Length | 2 | 71.47 | 142.94 |
| 60585K32 | Hand Brake for 1-1/2" & 3" Width Linear Bearing for T-Slotted Framing | 2 | 15.50 | 31.00 |
| 8982K931 | Multipurpose Aluminum (Alloy 6061) 90 Deg Angle, 3/8" Thick, 2" X 3" Legs, 4' Length | 1 | 59.90 | 59.90 |
| Total: | | | | \$1,052.87 |

Table 3.1: Cost Analysis for Upstairs Translation Table

3.4 Vacuum Pump Characteristics

Electric thrusters are designed to operate under high-vacuum conditions. The reasoning behind the expectation of a vacuum environment is twofold. First, electric propulsion is only feasible for missions occurring at a significant distance from the Earth's surface. With their high specific impulse and extremely low thrust, electric thrusters can be used to attain very high velocity changes for a spacecraft over a long period of time, but their thrust-to-weight ratios are less than one, meaning that they are incapable of providing sufficient force for a spacecraft to escape the surface of the Earth.

In addition, an electric thruster would be unable to operate in the presence of a dense ambient gas. Consider, for example, a typical electrostatic thruster. The velocities of the ions released by the thruster, called primary beam ions, are extremely high, usually at least 10 km/s but capable of exceeding 50 km/s. At such high speeds, the ions are deflected by local electromagnetic forces by only a small amount, so they continue in a relatively straight path away from the spacecraft. However, if the primary beam ions encounter a dense ambient gas, they will undergo charge exchange (CEX) collisions with the

surrounding particles. In a typical charge exchange collision, the beam ion transfers its charge to a neutral particle, but retains most of its momentum. The result is a fast-moving neutral particle and a slow-moving ion. The slow CEX ions follow nonlinear paths and may impinge upon the surface of the ion thruster, causing gradual damage.

Most ion sources, including the Kaufman ion source, which will be used in the bell-jar, are designed to operate in vacuum conditions. However, it is impossible to produce a perfect vacuum on earth. In practice, the diffusion pump which evacuates the bell-jar can establish a partial vacuum with a pressure as low as 1E-7 torr.

The recommended operating mass flow of the Kaufman ion source is between 3 sccm and 5 sccm (Commonwealth 13). Here sccm stands for standard cubic centimeter per minute. A mass flow of 1 sccm means that the amount of mass which flows through an area in one minute would occupy exactly one cubic centimeter at standard temperature (273.15K) and pressure (101,325 Pa). At these conditions, note that one cubic centimeter of gas corresponds to

$$n = \frac{PV}{RT} = \frac{(101,325Pa)(10^{-6}m^3)}{\left(8.3143 \frac{J}{mol-K}\right)(273.15K)} = 4.46159 \times 10^{-5} mol.$$

For argon, with a molar mass of 39.948 g/mol, 1 sccm then converts to

$$1sccm = \frac{\left(39.948 \frac{g}{mol}\right)(4.46159 \times 10^{-5})}{60s} = 3 \times 10^{-5} \frac{g}{s} = 3 \times 10^{-8} \frac{kg}{s}.$$

This means that the recommended operating mass flow range of the Kaufman source may be expressed as

$$9 \times 10^{-8} \frac{kg}{s} < \dot{m} < 1.5 \times 10^{-7} \frac{kg}{s}.$$

Now consider the pumping rate of the bell-jar's diffusion pump. The pump is a VHS-6 diffusion pump with an extended cold cap, which has advertised pumping rates of 2000 L/s for helium or 1600 L/s for air. Since the molar mass of argon is greater than the average molar mass of air, and since pumping rates in practice are often less than those advertised, the pumping rate for argon is 1000 L/s or one cubic meter per second. We can use this pumping speed to determine the mass flow exiting the chamber through the diffusion pump. If we define S as the pumping speed and ρ as the gas density in the chamber, then:

$$\dot{m} = \rho S.$$

Recalling the upper and lower limits on \dot{m} established by the ion source manual, and invoking the ideal gas law, we obtain:

$$9 \times 10^{-8} \frac{kg}{s} < \left(1 \frac{m^3}{s}\right) \left(\frac{P_{chamber}}{RT}\right) < 1.5 \times 10^{-7} \frac{kg}{s}.$$

We assume that the gases are at room temperature, and obtain the gas constant for argon by dividing the universal gas constant by the molar mass of argon to obtain:

$$9 \times 10^{-8} \frac{kg}{s} < \left(1 \frac{m^3}{s}\right) \frac{P_{chamber}}{\left(\frac{8.3143 \frac{J}{mol \cdot K}}{39.948 \frac{g}{mol}}\right) (298 K)} < 1.5 \times 10^{-7} \frac{kg}{s}.$$

Simplifying, we obtain:

$$0.005582 Pa < P_{chamber} < 0.0093033 Pa.$$

Finally, convert to torr in order to compare to the ideal operating pressures of the diffusion pump:

$$4.2 \times 10^{-5} \text{ torr} < P_{\text{chamber}} < 7 \times 10^{-5} \text{ torr}.$$

While this pressure range is acceptable for the diffusion pump, it is a greater pressure than we would like to use because of the possibility that gas particles at pressures in the range of $50 \mu\text{torr}$ might cause CEX collisions, threatening to damage the Kaufman ion source. Therefore our next objective is to run simulation software to predict the number of charge exchange collisions which are expected to occur.

Chapter 4: Ion Source Plume Modeling

Plume modeling is important to guide design of the stand due to thruster operating lifetime considerations as well as probe sizing. Analysis of plume from the Kaufman 3-cm ion source is performed using a particle-in-cell code *Plumpic*. We present in this chapter the basic elements of *Plumpic* and some preliminary results.

4.1 PLUMPIC Simulation of the Ion Source

In order to obtain a reliable estimate of the ion backflow, a particle-in-cell code *Plumpic* was used to simulate the operation of a 3-cm Kaufman ion source under the vacuum conditions described in section 3.4. The FORTRAN code was developed by Roy [1995] and used in ion thruster simulations. The term *plumpic* is a concatenation of “plume” and “PIC,” or Particle-In-Cell, and is the computational method used to predict ion plume characteristics. In essence, the PIC technique involves the creation of macroparticles, imaginary particles which each represent several million atoms or ions, and numerically solving Maxwell’s equations for these macroparticles. Prior to Roy’s work, the PIC technique had been established for use in plasma physics (Birdsall and Langdon, 1991; Hockney and Eastwood, 1988; Tajima, 1989).

Plumpic was originally developed to work alongside the ITPACK matrix solver package. Although ITPACK was only extensively tested with some f66 compilers and f77, the library was adapted to compile with the g77 compiler; the only changes needed involved the renaming of some ITPACK subroutines which conflicted with the names of intrinsic g77 routines.

By taking advantage of large improvements in computational resources over the past two decades, one may use this code to obtain accurate predictions of the ion plume properties. All of the calculations presented here were performed on the solar-3 cluster at WPI. The cluster utilizes 24 Intel® Xeon® 3.47 GHz CPUs. The longest computations performed involved 10,000 iterations of the *plumpic* routine and required less than one day to complete.

The input files used by Roy were adjusted to suit the bell-jar vacuum chamber conditions. For example, the ambient gas molecules in the chamber are expected to be argon, not oxygen or hydrogen as Roy simulated for thrusters in LEO or GEO. In an orbit, neutral, slow-moving propellant atoms do not accumulate around the thruster in any appreciable amount as they do in a vacuum chamber with a limited pumping speed. To be compatible with the pumping speed predictions of section 3.4, a background pressure of $50\mu\text{torr}$ was selected. The complete input file is included in the Appendix.

The outcomes from the PIC simulation are illustrated in Figs. 3.15-3.19 on the following pages. Fig. 3.15 illustrates a vector diagram of the CEX current density throughout the region surrounding an ion thruster. Here, X represents the axial direction and Y represents the transverse direction. A close-up view of the region directly surrounding the thruster exit is given in Fig. 3.16. Note that the CEX ions formed directly at the thruster exit, in the region immediately adjacent to $X=0.5\text{m}$, are attracted back toward the accelerator grid. CEX ions several millimeters farther out are accelerated away from the thruster if they are located close to the centerline; those farther away from the centerline are likely to be deflected away from the centerline, and occasionally may be attracted back toward the thruster body.

The backflow current density of CEX ions is illustrated in Fig. 3.17. A quartic fit of this data was performed using the *polyfit* routine from MATLAB. The results may be used to estimate the number of ions which impinge upon the thruster exit grid.

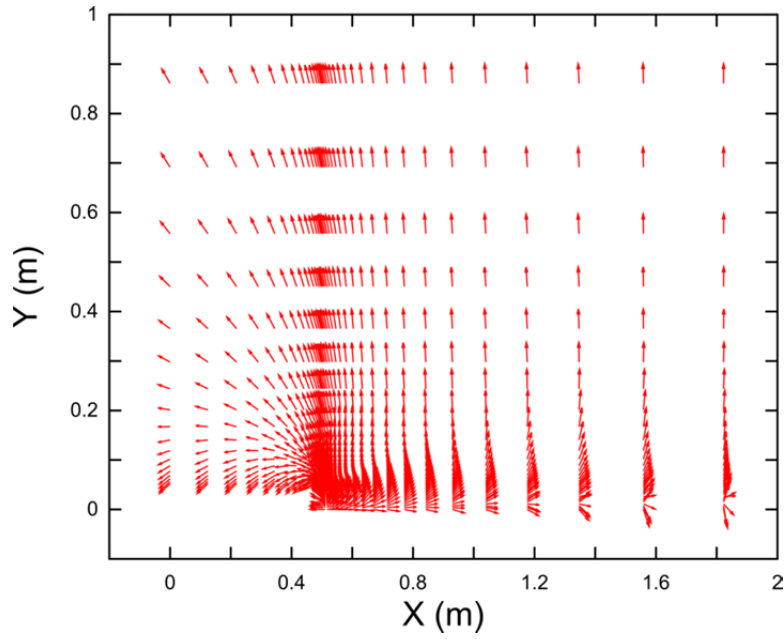


Fig. 3.15: Vector plot of CEX current density in a half-domain surrounding the electric thruster, which has an exit centered at (0.5m, 0.0m).

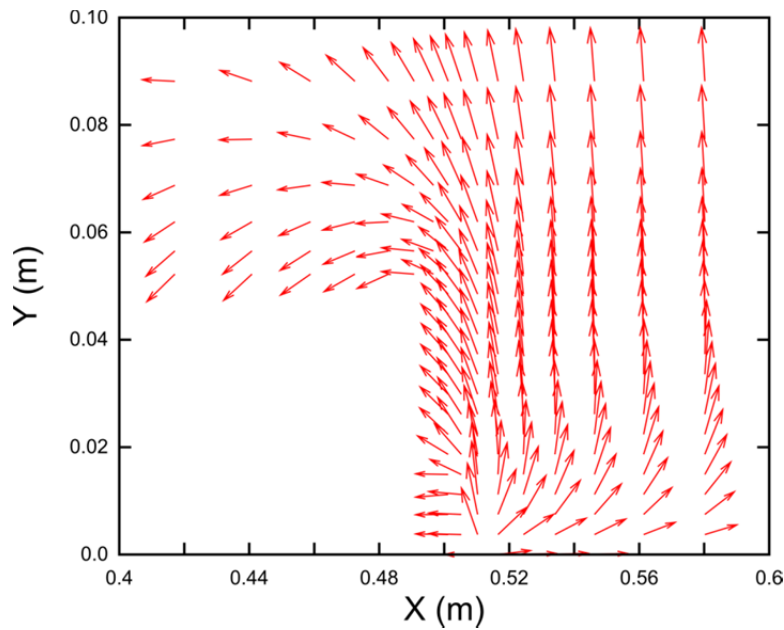


Fig. 3.16: A close-up view of the thruster exit from Fig. 3.15. Note that CEX ions generated due to collisions immediately beyond the accelerator grid are more likely to be deflected toward the grid than away from it, unlike ions generated in more distant regions.

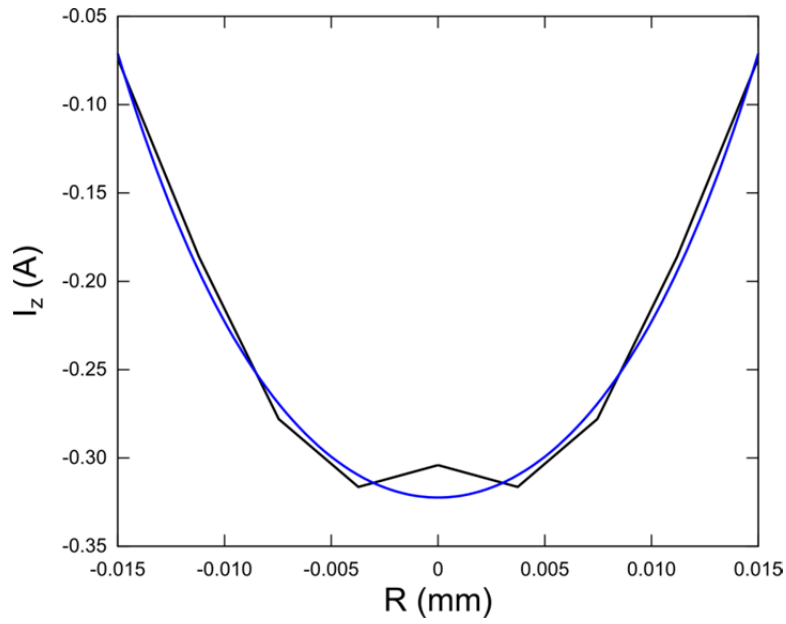


Fig. 3.17: Axial component of current density across the thruster exit, shown with a sample quartic fit generated using MATLAB's *polyfit* routine.

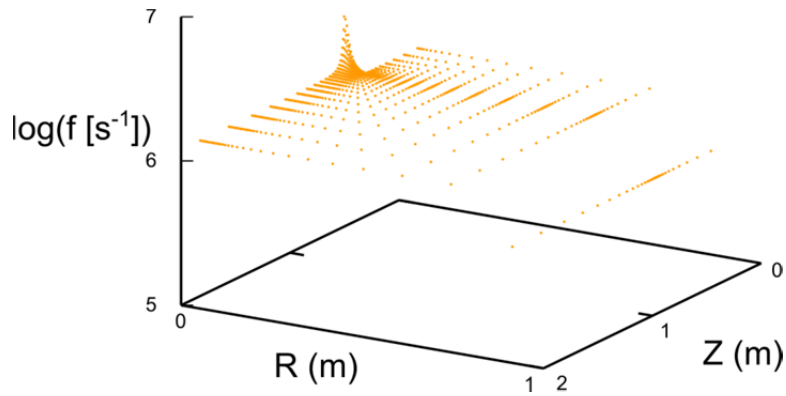


Fig. 3.18: Common logarithm of ion collision frequency in a half-domain immediately surrounding the ion source. Note a sharp spike located at the center of the thruster exit.

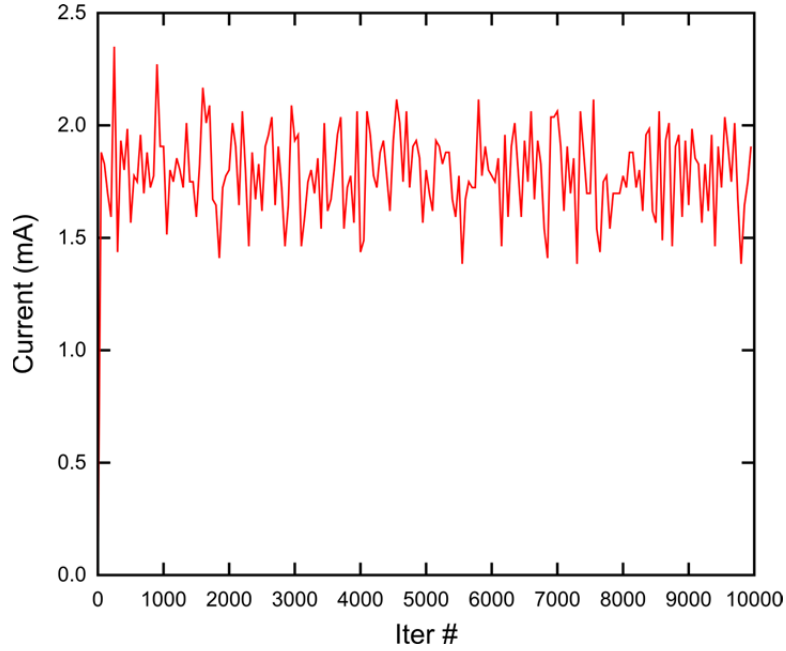


Fig. 3.19: CEX backflow current at various iterations of *plumpic*. The backflow current easily reaches steady state before the 1000th iteration.

The quartic fitting routine provided the following polynomial approximation to Fig. 3.17:

$$I_z(r) = P_1 r^4 + P_2 r^3 + P_3 r^2 + P_4 r + P_5,$$

where the five coefficients are approximately 963925.4 A m⁻⁴, 0, 90.04 A m⁻², 0, and -0.322447 A, respectively. To obtain an estimate of the overall current of ions impinging upon the accelerator grid, integrate the polynomial fit over the exit area:

$$I = \int_0^{2\pi} \int_0^{0.015} (P_1 r^4 + P_2 r^3 + P_3 r^2 + P_4 r + P_5) r dr d\theta$$

$$I = 2\pi \left[\frac{P_1 r^6}{6} + \frac{P_2 r^5}{5} + \frac{P_3 r^4}{4} + \frac{P_4 r^3}{3} + \frac{P_5 r^2}{2} \right]_0^{0.015}$$

For the given polynomial fit, the backflow current is approximately 0.0333mA. Assuming all ions have a single positive charge, the number of backflow ions may be calculated as:

$$n_{bkflow} = \frac{I}{e} = \frac{3.33 \times 10^{-5} \frac{C}{s}}{1.602 \times 10^{-19} \frac{C}{ion}} = 2.08 \times 10^{14} \frac{ions}{s}$$

The total number of ions which impinge on the accelerator grid is about a full order of magnitude smaller than that predicted by Roy [1995]; however, Roy was using NASA's 30-cm ion source to run simulations, not a small 3-cm source, so our result implies a number density of impinging ions about one order of magnitude higher than Roy's. However, this result is to be expected since we are using a lightweight atom (argon) as propellant in the simulation, and we include the effects of a considerable ambient gas pressure. When comparing the overall mass density of impinging CEX ions, we find that our simulation would suggest a density between 2 and 3 times that predicted by Roy due to differences in the propellant atomic mass. While this result suggests that the introduction of an ambient gas at 50 μ torr does affect the number of impinging ions in the simulation, the change is not large enough to discourage operation of the thruster.

The collision frequency of ions in the plume is illustrated in Fig. 3.18. In the area immediately surrounding the thruster exit, the frequency is about 10^6 collisions per second for the average particle. However, the velocity of the beam ions may be calculated as:

$$V_B = \sqrt{\frac{2e\Phi_B}{m_i}}$$

where Φ_B is the beam voltage, m_i is the ion mass, and e is the charge of an electron. By using argon and a beam voltage of 1000V, we predict an ion velocity of about 70 km/s.

The total backflow current is illustrated in Fig. 3.19. The portion of this beam current which impinges on the accelerator grid has already been discussed in the analysis of Fig. 3.17. The rest of the deflected CEX ions will impinge on other surfaces, most likely the walls of the vacuum chamber. Note that the current reaches a steady value before the 1000th iteration. In Roy [1995], the current doesn't reach a steady state for several thousand iterations. This may be due to the smaller domain needed to model the surroundings of the 3-cm Kaufman source, or the smaller number of macroparticles needed for the simulation.

Although *Plumpic* includes an electron temperature solver, the routine currently was not compiled. This may be due to the g77 compiler being used, or to errors in a separate input file for ITPACK solver parameters. A complete compilation of *Plumpic* will enable a better prediction of the energy of the impinging CEX ions, leading to an improved prediction of the potential damage they may inflict on the accelerator grid.

Chapter 5: Conclusions & Recommendations

The objective of this Major Qualifying Project was the design of two setups to be used in plasma plume experiments. The setups involved mounting of a Kaufman 3-cm ion source on a fixed stand and a translating plasma-diagnostics stand that could mount a Triple Langmuir Probe, Quadruple Langmuir Probe, or a Retarding Potential Analyzer. Two positioning systems are designed, one to fit the large vacuum chamber at WPI's HL 016, and the other to fit a smaller bell-jar vacuum chamber at WPI's HL 314. It was determined, due to cost efficiency, to design both, but only purchase parts and assemble the translation table for the smaller bell-jar vacuum chamber. The design was accomplished by using the SolidWorks computer aided design software. Structural analysis was accomplished using COMSOL software. The project involved ordering of parts and integration of the second setup.

The design of the setup for the large vacuum chamber was based on SolidWorks. Cost analysis provided alternatives to be considered in future designs. Static and dynamic loading analysis was not performed. Future projects may require the construction of a positioning system for the Large Vacuum Facility, but development of a translation table for a future group, whose exact needs are still undefined, is beyond the scope of this MQP.

The setup for the bell-jar vacuum chamber was significantly different than that of the large vacuum chamber. Its vertical orientation caused unacceptably large static deflections in the first few iterations of the design. After thorough reinforcement, static and dynamic analysis using COMSOL software demonstrated that the final design will experience less than one micron of static deflection, and less than four microns of

deflection when the probe is in motion. These deflections are an order of magnitude smaller than the uncertainty in the positioning of the advertised linear stages. In addition, the error due to probe position is expected to be dwarfed by any error due to probe misalignment or the operation of the TLP itself, which are typically the primary drivers of uncertainty in TLP measurements (Gatsonis et al, 2004).

Compared to previous translation tables used with the WPI vacuum facilities, the translation system outlined in this MQP offers an extra degree of freedom by incorporating two linear stages in conjunction with a single rotary stage. The direction of plasma flow is determined by the direction of TLP orientation which maximizes the measured current. The translation system outlined here is specifically designed to have the freedom to move the TLP to a position in a plane containing the centerline of an ion source or PPT and to rotate the TLP until the observed current reaches a maximum. Therefore, the design has both the flexibility and the positioning accuracy necessary to measure the magnitude of ion density, the electron temperature, and the direction of plasma flow. Immediately the design offers greater flexibility than models with a single translational and rotational degree of freedom, which typically require the assumption that ions flow in a simple conical pattern, radially outward from the center of the ion source exit plane (Flaherty et al, 2004).

Preliminary estimates of the plasma plume components from the Kaufman 3-cm plasma source were obtained using the particle-in-cell code *plumpic*. The simulations provide among other properties the number of charge-exchange ions impinging on the accelerator grid of the Kaufman ion source due to ambient gas in the chamber.

5.1 Recommendations

The process of designing a structure in SolidWorks to then import to COMSOL for analysis is very delicate. Complex geometries that are very easy to create in SolidWorks usually will give the user considerable trouble when attempting to mesh the structures in COMSOL. It is thus recommended that all geometries are kept as simple as possible. Primary load bearing structures, (like the upright double T-slot rails), may need to be redesigned with simplified cross-sections.

It is recommended that great care is taken when handling and operating the rotary and translational stages due to their high cost and required sensitivity. These stages are what enable movement of the probe in the plume, and experimentation without accurate operation of these stages will be nearly impossible.

Along with the structural analysis of the stand, which was outlined in Chapter 3, we recommend that a thermal analysis of the translation system be performed. The maximum recommended temperature of the lining between the purchased sliders and rails should be considered carefully when performing thermal analysis, as this is likely the most sensitive area to extreme temperature. The thermal expansion of aluminum, which is the primary building material in the stand, should also be analyzed.

Though TLP sizing and construction remains a task set for the future, our initial research highlighted their fragility. The orientation of all three of the tungsten wires must be maintained parallel to the highest degree. Ceramic casing for the wires is very brittle, but readily available for purchase.

One of the long-term goals of this MQP was to incorporate a Pulsed Plasma Thruster. However, as the scope of the project changed to incorporate a large overhaul of the existing selection of probe positioning systems, the analysis of a PPT became infeasible in the same time frame. Although the computational work outlined in Chapter 4 is well-suited to the adaptation of an ion thruster, the use of a pulsed plasma thruster would add a unique new dimension to the computational problem, since there would no longer be any steady state to which the solution could converge. Therefore, sizing a TLP for use with a PPT would require use of a PPT plume simulation code (Gatsonis and Yin, 2001). Time-dependent COMSOL analysis would likewise need to be expanded greatly.

Appendix

The input file used to generate the output shown in Figs. 3.15-3.19 is included here.

```
C *****
C * This is the input file for the hybrid PIC code, PLUMPIC *
C * Robie I. Samanta Roy, MIT SPPL/CASL *
C * Ion Thruster version (r-z) *
C *****

C All units in MKS, except for Te in eV
C Thruster specific items denoted by: *->
C CODE SWITCHES denoted by: (**)

C -----
C GEOMETRY ITEMS:
C NOTE: Y dimensions are HALF WIDTHS. (Y=r, X=z)
C This is the total length of the domain in X (m):
  XLEN = 2.0
C This is the half-width of the domain in Y (m):
  WID = 1.00
C This is the length of the thruster (or S/C) in X (m):
  THRLEN = 0.50
C This is the half-width of the S/C including thruster (m):
  THRWID = 0.05
C YSA is the length SA's extend above S/C (m):
  YSA = 0.0
C Solar Array potential drop (V):
  SADPHI = 28.0
C Length of shield extending above S/C top (m):
  SHLD = 0.0
C Plume Shield potential (V):
  SHLDPOT = 10.0

C *->Beam radius (m): (Make sure BEAMWD <= THRWID, THRWID+YSA < WID)
  BEAMWD = 0.015
C *->Divergence angle of beam (degrees):
  PI = 4.*ATAN(1.)
  DIVANG = (20.0)*PI/180.0
C NOTE: B.C.'s on potentials set in bcond.f

C Stretching factors for grid at: x=0: X0, x=L: XL, y=+/-YWID: YW.
C This is the amount the grid cells are stretched at the far boundaries
C compared to the grid cells directly in front of the thruster
C (the smallest).
  X0 = THRLEN/BEAMWD
```

```

XL = (XLEN-THRLEN)/BEAMWD
YW = WID/BEAMWD
C Set the size of the smallest grid cell in a region in terms of no.'s
C of reference Debye lengths.
C For 0<x<THRLEN:
  XNCELL1 = 10.
C For THRLEN<x<XLEN:
  XNCELL2 = 10.
C For 0<y<|THRWIDTH|:
  YNCELL1 = 10.
C For |THRWIDTH|<y<|YWID|:
  YNCELL2 = 10.
C These parameters offer the tradeoff between memory and resolution.

C -----
C PLASMA (THRUSTER AND BACKGROUND) ITEMS:
C (**)IVARTEMP is a switch for variable electron temp. model: 0=Off,1=On
C (Off means isothermal Boltzmann electrons.)
  IVARTEMP = 1
C (**)IFLTPOT is a switch for floating s/c potential: 0=Off,1=On
C (Off means set s/c potential to be fixed value SCPOT (V))
  IFLTPOT = 0
  SCPOT = -5.
C *->Beam current (A):
  BMCUR = 0.1
C *->Beam ion exit velocity (m/s):
C Can relate to beam potential V_b(Volts): sqrt(2eV_b/xmion)
C BEAMV = 41762.
C BEAMV = 69497.
C *->Accel grid potential (V):
  PHIACEL = -100.
C *->Propellant utilization efficiency:
  PREFE = 0.88
C *->Mass of ion (kg/mole): C-60=0.72066, Hg=0.20059, Xe=0.13129
C XMION = 0.13129/6.02214E23
C XMION = 0.039948/6.02214E23
C *->CEX cross-section (m^2):
C (**)MAKE SURE APPROPRIATE E-N CROSS-SECTION IS SET IN colfreq.f !
C This is for Xe: (fast ion + slow neutral -> fast neutral + slow ion)
C SIGMA = (-0.8821277*LOG(BEAMV)+15.12616)**2*(1.E-20)
C SIGMA = 3.963E-19
C This is for Hg:
c SIGMA = (-0.9096784*LOG(BEAMV)+15.86866)**2*(1.E-20)
C *->Electron TE (eV) and Ion temperatures TI (K):
C TE is a ref. quantity, and can be max. at thruster exit.
  TE = 5.0

```

TWALL = 500.
 TI = TWALL/11604./TE
 EC = 1.60218E-19
 EPSO = 8.85419E-12
 BK = 1.38066E-23
 CION = SQRT(EC*TE/XMION)
 VTHERM = SQRT(3.*BK*TWALL/XMION)
 VTE = SQRT(EC*TE/9.11E-31)
 AREA = PI*BEAMWD**2
 RO=BEAMWD/(DIVANG*COS(DIVANG/2.))
 PHIC = 1. - 2.*COS(DIVANG)/DIVANG**2 - 2.*SIN(DIVANG)/DIVANG +
 + 2./DIVANG**2
 ALPHA = BMCUR/(2.*PI*RO**2*EC*BEAMV*PHIC)
 C MAX Beam ion density (#/m^3): (Can also just specify)
 C (**)MAKE SURE APPROPRIATE BEAM MODEL IS SET IN beam.f !
 C For spherical parabolic:
 DENBEAM = ALPHA
 C For gaussian distribution:
 c CORR = 0.6
 c DENBEAM = CORR*BMCUR/((0.5)*PI*BEAMWD**2*EC*BEAMV)
 C This is fraction of beam density used for reference density:
 C (Since CEX density<Beam density, no need for such high reference)
 DENFRAC = 0.08
 DENSO = DENFRAC*DENBEAM
 WPI = EC*SQRT(DENSO/(EPSO*XMION))
 WPE = WPI*SQRT(XMION/9.11E-31)
 DEBYEL = CION/WPI
 C Neutral gas density (#/m^3):
 C *->Neutral flow-through area fraction:
 FLONAR = 0.24
 CBAR = SQRT(8./PI*BK*TWALL/XMION)
 DENSNM = 4.0*BMCUR/(EC*AREA*FLONAR*CBAR)*(1.-PREFF)/PREFF
 C Background tank pressure (for ground tests) (torr) and temp (K):
 C We assume same gas as thruster propellant. Density in (#/m^3):
 C With PLUMPICMO, set BKGPRES = 0.0
 BKGPRES = 0.00005
 TBKG = 300.
 VTBKG = SQRT(3.*BK*TBKG/XMION)
 BKGDEN = BKGPRES*(101325./760.)/(BK*TBKG)
 C Background plasma density (#/m^3): (i.e. GEO and LEO)
 DENINF = 1.E+9
 C Ratio of background to ion reference density:
 DENRAT = DENINF/DENSO
 C Background electron temperature (eV) for temperature eqn.:
 TEINF = 0.1
 C *Quantities for s/c floating potential computation:

C Ambient electron temperature (eV) for floating potential:
 C (Usually the same, but may be different in GEO)
 TEAMB = 1.0
 C Ambient ion mass (kg/mole): LEO: O = 0.016, GEO: H = 0.001
 C XMAMB = 0.016/6.02214E23
 XMAMB = 0.039948/6.02214E23
 C S/C velocity through plasma (m/s) - for ion ram current:
 VSC = 0.
 C *->SPUTTERED GRID MATERIAL DATA: (Mo here)
 C Mass of Mo:
 XMASSMO = 0.09594/6.02214E23
 C Most probable ejection energy (eV):
 ENEJMP = 5.
 C Most probable ejection velocity (m/s):
 VELEJ = SQRT(2.*(EC*ENEJMP)/XMASSMO)
 C Density of neutral moly at thruster exit (m^-3):
 C (Estimate from either impingement current or mass loss)
 DENMOLY = 3.25E13
 C Mo-Xe CEX cross section (m^2) (fairly energy independent):
 CEXMOLY = 6.E-20

 C -----
 C SIMULATION ITEMS:
 C No. of real particles per CEX ion macroparticle:
 C ZCEX = 350000000.
 ZCEX = 3500000.
 C Scaling in x&y-dirs:
 XSCALE = DEBYEL
 YSCALE = DEBYEL
 C Max. time step: wpi*dt=0.2; computer variable is non-dim wrt wpi
 DT = 0.2
 C Timestep no. to write files: potentials, densities, vector plots:
 IOFTIME = 500
 C Timestep no. to write particle files:
 IOPTIME = 500
 C Timestep no. to write files: diagnostics like total energy:
 IDIAG = 200
 C Timestep no. to write restart file:
 IDUMP = 500
 C Minimum no. of particles to create each timestep:
 NPLIM = 100

References

- 1) Asselin, Daniel Joseph, 2011, "Characterization of the Near-Plume Region of a Low-Current Hollow Cathode." M.S. thesis, Department of Mechanical Engineering, Worcester Polytechnic Institute.
- 2) Commonwealth Scientific Corporation, 1984, "Operating and Maintenance Instructions for 3cm ion Source Model II."
- 3) Flaherty, A., Hathaway, R., Martin, J., and Rosen, D., 2004. "Design and Construction of a Probe Positioning System for Pulsed Plasma Thruster Diagnostics." Major Qualifying Project, Department of Mechanical Engineering, Worcester Polytechnic Institute.
- 4) Partridge, James, 2008, "Development and Implementation of Diagnostics for Unsteady Small-Scale Plasma Plumes." Ph. D. thesis, Department of Mechanical Engineering, Worcester Polytechnic Institute.
- 5) Roy, Robie I. Samanta, 1995, "Numerical Simulation of Ion Thruster Plume Backflow for Spacecraft Contamination Assessment." Ph. D. thesis, Department of Aeronautics and Astronautics, Massachusetts Institute of Technology.
- 6) Sutton, G. and Biblarz, O., "Rocket Propulsion Elements." New Jersey: John Wiley and Sons, 2010.
- 7) Gatsonis, N.A, Byrne. L., Zwahlen, J., Pencil, E., Kamhawi, H., "Current Mode Triple and Quadruple Langmuir Probe Methods with Applications to Flowing Pulsed Plasmas," *IEEE Transactions on Plasma Science*, 32, 5, pp. 2118-2129, October 2004.
- 8) Tajima, T., *Computational Plasma Physics: With Applications to Fusion and Astrophysics*, Addison-Wesley, NY, 1989.
- 9) Hockney, R.W. and Eastwood, J.W., *Computer Simulation using Particles*, Adam Hilger, Bristol, 1988.
- 10) Birdsall, C.K. and Langdon, A.B., *Plasma Physics via Computer Simulation*, Adam Hilger, Bristol, 1991.
- 11) Partridge, J., and Gatsonis, N.A., "Characterization of High Density Flowing Plasmas Using a Directional Micro-Retarding Potential Analyzer," IEPC 2005-170, 29th International Electric Propulsion Conference, Princeton, NJ, November 2005.
- 12) Gatsonis, N. A., and Yin, X., "Hybrid (particle-fluid) modeling of pulsed plasma thruster plumes" *Journal of Propulsion and Power*, 17, 5, pp. 945-958, Sept.-Oct. 2001.